Accepted Manuscript

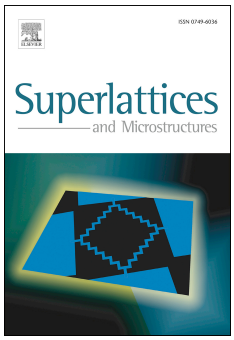

Theoretical framework for performance evaluation of silicon quantum dot solar cell under low concentration illumination

Zeel Purohit, Brijesh Tripathi

PII: S0749-6036(16)31184-3

DOI: 10.1016/j.spmi.2016.10.036

Reference: YSPMI 4581

To appear in: *Superlattices and Microstructures*

Received Date: 10 October 2016

Accepted Date: 12 October 2016

Please cite this article as: Z. Purohit, B. Tripathi, Theoretical framework for performance evaluation of silicon quantum dot solar cell under low concentration illumination, *Superlattices and Microstructures* (2016), doi: 10.1016/j.spmi.2016.10.036.

This is a PDF file of an unedited manuscript that has been accepted for publication. As a service to our customers we are providing this early version of the manuscript. The manuscript will undergo copyediting, typesetting, and review of the resulting proof before it is published in its final form. Please note that during the production process errors may be discovered which could affect the content, and all legal disclaimers that apply to the journal pertain.

ACCEPTED MANUSCRIPT

Theoretical framework for performance evaluation of silicon quantum dot solar cell under low concentration illumination

Zeel Purohit, Brijesh Tripathi*

Department of Science, School of Technology, Pandit Deendayal Petroleum University, Gandhinagar - 382007 (India)

*Corresponding Author: Ph: +91-79-23275455, Fax: +91-79-2327-5030, Email: brijesh.tripathi@sse.pdpu.ac.in

ABSTRACT

This article describes a silicon quantum dot (Si QD) solar cell with absorption enhancement due to quantum-confinement in the front-side emitter region, which helps in the improvement of the short-circuit current density. The Si QD solar cell is theoretically mimicked using an equivalent circuit to account the possible recombination losses under low concentration illumination. The electrical output is estimated using proposed theoretical model by considering the fundamental properties of intrinsic Si reported in the literature. An increase of ~7.5% in generated current density is observed due to extra absorption of incident radiation through Si QD, which is in accordance with the experimental findings. The performance of Si QD/c-Si solar cell has been studied with respect to low concentration illumination, wherein with increasing CR from 1 sun to 5 suns, the short circuit current density increases from 29.4 to 147.2 mA/cm^2 and the open circuit voltage increases from 0.565 to 0.609 V. This study provides a theoretical framework for design optimization of a future Si QD solar cells to achieve better performance of the device.

KEYWORDS: Quantum heterostructure, silicon quantum dot solar cell, quantum efficiency, low concentration illumination

1. INTRODUCTION

Silicon (Si) is the most abundant, nontoxic material on the earth surface, which is leading the photovoltaic (PV) market since the beginning of the PV technology [1]. In past few decades, the Si wafer thickness has decreased from 400 μm to the current 180 μm and the decreasing trend is continuing with recent attempts towards 18 μm, i.e. 1/10 of the current thickness [2, 3]. For reducing the thickness, kerf-less wafering approaches [4] are currently being commercialized by various industries, e.g. Direct Gas to Wafer (CrystalSolar [5]), Direct Wafer (1366Technologies [6]) and NexWafe [7]. However, the reduced wafer thickness presents a major challenge to maintain a high efficiency due to significant decrease in the light absorption at the longer wavelengths, especially when the wafer thickness is reduced to below 50 μm [8]. With reduction in thickness, an increase in light absorption is desirable to maintain a high short-circuit current density of the solar cell [9]. The decreased light absorption has been attempted through various light trapping schemes including nanotexturing [10, 11] and plasmonics [2, 12]. A review of light trapping schemes is presented by Glunz [13], which includes classical approaches such as pyramids and internal reflection layers and recently explored concepts including plasmonics nanostructures and diffractive optics. With decreasing thickness of Si wafer, the importance of a-Si:H/c-Si heterojunction solar cells is increasing due to their high efficiency potential, low temperature coefficient, and low production cost [14]. Recently, a-Si/c-Si heterostructure based solar cells have been attempted theoretically with innovative ideas of inserting quantum wells (QW) [15] as well as experimentally by various solar PV researchers [16-21]. The use of QW falls under the third generation solar PV technologies, which have been extensively explored to overcome the material limitations of Si wafer-based solar cell technology and efficiency limitations of thin film solar cell technologies in order to have affordable PV technology [22,

23]. Further, there have been extensive fundamental and applied investigations in the area of third generation solar cells, which are designed to improve the efficiency of solar cells by adopting novel ways such as use of QW or quantum dots (QD) for enhanced absorption of solar spectrum [24-36]. Towards the development of QD solar cells, the composite materials consisting of Si nanocrystals embedded in a dielectric matrix have attracted considerable interest [37-43]. Moreover, the extent of quantum confinement that is observed in Si nanoparticles of a few nanometers is very prominent to engineer the material bandgap [43, 44-45]. Silicon nanocrystals of very small size (<∼7 nm in diameter) behave as quantum dots (QDs) due to the three-dimensional quantum confinement of carriers [46-47]. These reasons indicate the suitability of Si to explore the third generation objectives as active material of solar cells. It is important to note that there are various approaches to use QDs for improving the spectral absorption, which result in enhanced electrical output. In one of the approaches, Löper et al. [48, 49] have used Si QDs in the absorber region of p-i-n solar cells in order to obtain a higher voltage. The investigations carried out in this article focus on achieving a higher efficiency Si solar cell using a different approach wherein Si QDs are used for quantum-confinement in the front-side emitter region to improve the short-circuit current density as reported in Ref. [46]. This article reports for the first time a semi-analytical theoretical model to explore the effect of QD layer on the electrical performance of a Si solar cell which includes the role of recombination mechanisms. Further, enhanced spectral absorption because of the presence of Si QD layer is reported and design parameters are discussed. The effect of inserting QD layer on the electrical performance parameters of QD solar cell, such as short-circuit current density (J_{SC}), open-circuit voltage (V_{OC}), maximum output power (P_{max}) and the conversion efficiency (η) is reported.

2. THEORETICAL MODEL USING EQUIVALENT CIRCUIT

The Si quantum dot solar cell is modeled as a P-N junction device, which can be fabricated by depositing phosphorus-doped Si QDs in a SiO_2 matrix (N-layer) on p-type crystalline Si substrates (c-Si) [46] as shown in Fig. 1 with corresponding band-diagram shown in Fig. 2. The incident solar radiation is directly converted into electricity due to photovoltaic action of P-N junction and produces a non-linear current-voltage characteristic response. The non-linearity mainly arises due to the recombination of photo-generated carriers through different mechanisms of photo-generated carrier loss, which have been described by different researchers [50-51].

In a solar cell, the energy loss mechanisms related to photo-generated carriers include, (1) thermalization loss: photo-generated carriers move from initial excited states to the respective band edges, (2) spatial relaxation: the photo-generated carriers are swept along the band edges to the contacts, (3) radiative recombination of electron-hole pair, (4) Shockley-Read-Hall, Auger, and surface recombination, (5) series and shunt resistances. A two-diode model is proposed as an equivalent circuit for Si QD solar cell as it helps in explaining the mentioned loss mechanisms (Fig. 3) [52].

Diode 1 describes the rectifying behavior of a solar cell, which conducts the current arising from the diffusion of minority carriers in the quasi neutral regions of the solar cell. Diode 2 describes the recombination losses, which includes defect-induced charge recombination losses in the depletion region. The terminal equation for the current-voltage characteristics of the QD solar cell using equivalent circuit shown in Fig. 3 is given by [51-54]:

$$I = I_{PH} - I_{D1} - I_{D2} - (V + I\mathrm{R_S})/\mathrm{R_{SH}} \quad (1)$$

Assuming superposition principle ($I_{PH} = I_{SC}$, where, I_{PH} represents the photo-generated current density and I_{SC} represents the short-circuit current) [55], the photo-generated current density I_{PH}

is equal to '$q\Phi$', where q represents the electron charge and Φ represents the photon flux absorbed by the QD layer and base materials and expressed as [56-57] by replacing width of the confining layer, L_z by $f_{QD}V/A$ with the assumption that the reflection from the top surface is zero:

$$I_{PH} = q\Phi \times CR = CR \times \int_{\lambda_W}^{\infty} qF(\lambda)\left[1 - \exp\left(-\alpha_B(\lambda)W - N_{QD}\alpha_{QD}(\lambda)f_{QD}V/A\right)\right] d\lambda \quad (2)$$

where, CR represents the concentration ratio, $F(\lambda)$ represents the incident photon flux per nanometer from Air Mass 1.5 Global (1000 Wm^{-2}, AM1.5G) solar spectrum [58], $\alpha_B(\lambda)$ and $\alpha_{QD}(\lambda)$ represent the absorption coefficient of base material (c-Si) and QD material respectively, W represents the width of absorbing c-Si material, N_{QD} represent the number of QD layers (described in the next section), f_{QD} represents the number density of the QDs embedded in the dielectric layer, V represents the volume of a cubic QD, and A represents area of the solar cell. The absorption coefficient of the base material (c-Si) is referred from Green and Keevers [59]. The calculation of QD absorption coefficient, $\alpha_{QD}(\lambda)$ is described in detail in the next section.

The diode current density under forward bias can be expressed in terms of the voltage *V* [52]:

$$I_{D1} = I_i\left\{\exp\left(\frac{q(V+IR_S)}{nk_BT}\right) - 1\right\} \quad (3)$$

$$I_{D2} = I_r\left\{\exp\left(\frac{q(V+IR_S)}{mk_BT}\right) - 1\right\} \quad (4)$$

where I_{D1} and I_{D2} represent the current densities of diode 1 and 2, n and m represent the corresponding ideality factors and I_i and I_r represent the dark saturation currents of rectifying and recombination diode respectively, k_B represents Boltzmann's constant, T represents absolute temperature, q represents electron charge, R_S represents the series resistance and R_{SH} represents the shunt resistance.

The open-circuit voltage (V_{OC}) and fill factor (FF) of a Si QD solar cell under low concentration illumination is expressed by [60] under ideal conditions, i.e. $R_S \rightarrow 0$ and $R_{SH} \rightarrow \infty$ with an assumption that I_i ($\approx I_0$) is dominant around the V_{OC} [61]:

$$V_{OC}(CR) = \frac{k_B T}{q} \ln\left(\frac{I_{PH} \times CR}{I_0} + 1\right) \quad (5)$$

$$FF(CR) = 1 - \frac{v_t}{V_{OC}(CR)} \ln\frac{V_{OC}(CR)}{v_t} - \frac{I_{PH} R_S}{V_{OC}(CR)} \quad (6)$$

where, I_0 represents the dark saturation current density [62] and v_t represents thermal voltage (k_BT/q). The maximum power output of LCPV module is related to the I_{SC} and V_{OC} by [60]:

$$P_{MAX} = FF \times V_{OC} \times I_{SC} \quad (7)$$

The efficiency of the solar cell in relation with the P_{MAX} is given by [60]:

$$\eta = P_{MAX}/(A \times P_{in}) \quad (8)$$

A is the area of solar cell and P_{in} is the incident solar radiation (AM1.5G, 1000 Wm^{-2}).

The characteristic parameters of the solar cell, i.e. a series resistance and the shunt resistance are dependent on the semiconductor fabrication process and can be calculated by the slope of current-voltage characteristic curve near V_{OC} and I_{SC} respectively. Based on the theoretical model described above, the QD Si solar cell is simulated using MATLAB/Simulink.

3. OPTICAL ABSORPTION CALCULATION

For the optical absorption calculations, it is assumed that, the QD is cubic in shape (as per available literature [63]) and distributed in a SiO_2 matrix in a regularly spaced array as shown in Fig. 1. The cubic dot dimensions are defined as L_x, L_y, and L_z and the separation between dots is S_x, S_y, and S_z in the coordinate directions x, y and z respectively. The QD layer is defined as a dielectric layer with embedded QDs with the thickness calculated as $L_z + S_z$. Figure 4 shows the

notations used for the calculation of the density of states (DOS) and the absorption coefficient due to the quantum confinement of the charge carriers in the discrete energy levels.

The effective energy band gap of QD is represented by $E_{eff,}$ which is created by embedding the Si QD with an energy band gap, E_{QD} within the dielectric material (SiO_2) with an energy band gap of E_{SiO_2}. The conduction band offset is represented as ΔE_c and the valence band offset is represented as ΔE_v. The values of the E_{QD}, E_{SiO_2}, ΔE_c, ΔE_v and the corresponding effective masses of electrons and holes required for the calculations are listed in Table 1.

The energy levels of the Si QD conduction band with respect to the valence band edge of the dielectric material are represented from E_1 to E_n, where the number of the levels is dependent on the size of the QD. The calculated values of energy levels are listed in Table 2 for the Si QD size ($L_x \times L_y \times L_z$) of $5\times5\times5$ nm^3.

The energy levels and DOS are evaluated using following equations to calculate the absorption coefficient of QD embedded within SiO_2 matrix. The DOS is calculated using following equation [65]:

$$\rho_r^{0d} = \sum_i \delta(E - E_i) \tag{9}$$

where, ρ_r^{0d} represents the DOS of QD, where δ represents the Dirac delta function, E represents energy of incident photon and E_i represents the energy difference of i^{th} (i = 1, 2, …, n) electron and ground hole energy states in a QD. The Dirac delta function is modelled using a Lorentzian of finite width given by [65] to calculate the DOS:

$$\delta(\mathrm{E} - \mathrm{E_i}) = \frac{1}{\pi} \frac{\sigma}{(\sigma^2 - (\mathrm{E} - \mathrm{E_i})^2)} \tag{10}$$

where, σ is a parameter with the same dimensions as the argument of the delta function, which gives the width of the Lorentzian. In reference [63], Fig. 12 presents the order of DOS as 10^{28} $m^{-3}eV^{-1}$ for Si QD, which is calculated for one energy miniband, whereas using Eq. (9) and Eq.

(10), the DOS can be estimated for all the minibands of the QD with respect to the energy levels listed in Table 2.

The energy eigen value, E_i is found by searching for the root in [66]:

$$\sqrt{\frac{2m^*_{Be}(\Delta E_c - E_i)}{\hbar^2}} = \frac{m^*_{Be}}{m^*_{We}}\sqrt{\frac{2m^*_{We}E_i}{\hbar^2}}\tan\left(\sqrt{\frac{2m^*_{We}E_i}{\hbar^2}}\left(\frac{L_z}{2}\right)\right) \quad (11)$$

The effective energy band gap, E_{eff} is calculated by adding the energy band gap of Si QD with electron and hole energy of confined energy states of a QD using Eq. (11). The energy band gap of Si QDs with particle size (L_z) in the range of 4-9 nm embedded in SiO_2 lies in the range of 1.18-1.47 eV [67], which has been verified by recent study [37]. The DOS is calculated to be of an order of 10^{28} $m^{-3}eV^{-1}$ as plotted in Fig. 5, which matches well with the order of the data reported in the literature [63]. The wavelength in Fig. 5 corresponds to QD conduction band energy levels with reference to ground energy level of the holes with an uncertainty of ± 5 nm. Further, the absorption coefficient of embedded QD structure is calculated on the basis of interband optical transitions with following assumptions: (1) the band structure of the QD is completely filled with electrons in the valence band and empty in the conduction band, (2) the band structure does not incorporate the defect states.

The energy dependent interband absorption coefficient of the QD structure, α(E) is calculated using following expression [66], where the density of states of a quantum well is replaced by that of a QD:

$$\alpha(E) = C\left|\hat{e}.\vec{P}_{CV}\right|^2 \rho_r^{0d} \quad (12)$$

where, $C = \pi q^2\hbar/n_r c\varepsilon_0 m_0^2 E$; where e represents electron charge, n_r represents the refractive index of Si, c represents the speed of light in vacuum, ε_0 represents the electrical permittivity of electron in vacuum, m_0 represents electron rest mass, and $\left|\hat{e}.\vec{P}_{CV}\right|^2$ represents the optical matrix

element of Si [68]. The values of these parameters are listed in Table 3 for the calculation of energy dependent absorption coefficient.

The charge carrier confinement in a QD quantizes their energies in to a series of minibands, giving a distribution of DOS as shown in the Fig. 5. A similar distribution of absorption coefficient is observed with the maximum absorption value of ~7×10^5 cm^{-1}. Further, the size distribution of Si QDs can affect the absorption behaviour in the near-gap region as reported by Lee et al. [69], which shows blue-shift of absorption due to quantum confinement in smaller QDs. However, in the same article Lee et al. [69] reported the possibility of red-shifting because of strong absorption from the larger QDs with smaller energy gaps. In another article, Mirabella et al. [70] have reported that the density of Si-Si bonds is likely to affect the joint density of states and thus enhances the photon absorption probability and provided a clear evidence of an enhanced light absorption in quantum confined Si QD.

4. RESULTS AND DISCUSSION

The c-Si has an indirect band gap, which favors non-radiative recombination in the material, which must be considered for the performance evaluation. The current-voltage characteristics calculation is done to determine the effect of QD layer in a Si QD solar cell by including the effect of radiative and non-radiative recombination. On the basis of available literature [25], the dark saturation currents of rectifying and recombination diodes can be expressed as:

$$I_i \propto I_0(1 + r_R\beta) \tag{13}$$

$$I_r \propto r_{NR}\alpha \tag{14}$$

where, I_0 represents the dark saturation current density [71], r_R is radiative enhancement ratio which represents the fractional increase in the intrinsic region radiative recombination due to the

presence of the QD, β is the ratio of the current required to feed radiative recombination in the intrinsic region at equilibrium to the usual reverse drift current resulting from minority carrier extraction, r_{NR} is the non-radiative enhancement ratio which represents the fractional increase in the intrinsic region non-radiative recombination due to the presence of the QD, n and m represent diode ideality factors for radiative and non-radiative recombination respectively (for an ideal case n = 1 and m = 2), α represents the ratio of current required to feed non-radiative recombination in the intrinsic region at equilibrium, and Φ is the net flux of incident photons absorbed by the Si QD and base material. The dependence of β, r_R, α and r_{NR} on the intrinsic parameters of the solar cell material can be written as [25]:

$$\beta \propto Bn_i^2/I_0 \tag{15}$$

$$r_R \propto f_{QD}\left[\gamma_B\gamma_{DOS}^2\exp(\frac{\Delta E}{nk_BT}-1)\right] \tag{16}$$

$$\alpha \propto An_i \tag{17}$$

$$r_{NR} \propto f_{QD}\left[\gamma_A\gamma_{DOS}\exp(\frac{\Delta E}{mk_BT}-1)\right] \tag{18}$$

where, B represents radiative recombination coefficient [72], n_i represents intrinsic carrier concentration [73], f_{QD} represents the fraction of the N-layer volume replaced by QDs, γ_B represents the ratio of recombination coefficient QD material to barrier material, γ_{DOS} represents the DOS enhancement factor, ΔE represents the energy difference between the band gaps of barrier material (E_{SiO_2}) and QD material (E_{QD}), A_B represents non-radiative recombination coefficient which is equal to the reciprocal of non-radiative carrier lifetime (τ_B), and γ_A represents the ratio of non-radiative carrier lifetime of barrier material to the QD material. The values of parameters required to explore the dependence of these terms on the intrinsic properties of the material are listed in Table 4. The radiative and nonradtive mechanisms of energy transfer from the QDs to the underlying Si have been studied by other researchers using

photoluminescence decay method [75]. In the Si QD solar cells, nonradiative energy transfer is accompanied with radiative transfer. Existing literature reports that the nonradiative energy transfer is inversely proportional to the distance of QD from the underlying Si surface (given as $\propto 1/(distance)^4$) [75]. The ratio of radiative to nonradiative recombination rate is related to the quantum yield (QY) by following relationship [76]: QY = $r_R/(r_R + r_{NR})$, which remains ~0.3 for the studied system [75]. The rate of non radiative energy transfer to the underlying Si remains ~1.6 times faster than the rate of radiative energy transfer [75]. The values of I_i, and I_r are listed in Table 5 for generating the I-V characteristics.

Further, the quantum efficiency of the Si QD solar cell is calculated with respect to the wavelength (λ) using following expression [77]:

$$QE(\lambda) = \frac{I_{PH}(\lambda)}{qF(\lambda)} \tag{19}$$

The quantum efficiency depends on the optical properties and layer thicknesses of the solar cell, which is included in the calculation of the photo-generated current.

4.1. Quantum efficiency

The quantum efficiency of a Si QD solar cell has been modelled to find the generated photo-generated current density. The room temperature escape probability for photoexcited charge carriers in QD is assumed to be unity [78]. Using the knowledge of the optical and charge carrier transport properties of the Si material as listed in previous sections, the photogenerated current density and corresponding quantum efficiency is calculated with respect to the wavelength of incident photons as shown in Fig. 6(A) and 6(B) respectively. The lower curve in Fig. 6(A) and 6(B) represents the photogenerated current density and quantum efficiency respectively of the base solar cell made of c-Si material. The value of number of QD layer equal to zero means the absorbing region of the device is entirely the c-Si material having a band gap of 1.1 eV, which

corresponds to the wavelength >1100 nm. The integration of the lower curve (N_{QD} = 0) with respect to the wavelength (Fig. 6(A)) yields the photogenerated current density of 27.44 mA/cm^2 (with device thickness W equal to 18 μm) for a baseline c-Si solar cell without QD for an ideal case of unit collection efficiency of generated charge carriers without any recombination loss. For the ideal case, Fig. 6(B) shows 100% conversion of incident photons in to the electron-hole (e-h) pair in the wavelength range of 350-1100 nm. Under similar conditions, the addition of 25 QD layers on top of the c-Si solar cell with f_{QD} equal to ~4×10^{12} cm^{-2} in each layer leading to the effect of quantum confinement, the quantum efficiency curve shows spikes of e-h pair generation corresponding to the mini-bands of energy confined in three dimensions. The order of calculated f_{QD} (on the basis of $f_{QD} = \mathrm{L_z} \times \mathrm{A/V}$) is in agreement with the experimental number density of QD in Si solar cell as reported in literature [43, 79-80]. The extended area under the curve due to presence of QD adds up more e-h pair in the photo-generated current density of the solar cell. The integration of this curve (N_{QD} = 25) with respect to the wavelength yields a higher photogenerated current density of ~29.5 mA/cm^2, which is significantly higher compared to the baseline current density. An increase of over 7.5% in generated current density is registered due to extra absorption of incident radiation through QD, which is in qualitative agreement with experimental findings [75, 81]. Even though Park et al. [81] show that the 3 nm QD gives best performance, but an improvement is expected with even 5 nm QD as compared to the baseline. Here in this article, the improvement in current density is calculated as ~7.5% with 5 nm QD, whereas an improvement in the current density of ~18% is presented by Dutta et al. [75] with 2 nm QD (note that Park et al. [81] have not studied 2 nm QDs). This comparison of theory and experiment indicates that the 3 nm QD may be superior to 5 nm QD, which is experimentally observed by Cho et al. [46].

4.2. Current-voltage characteristics

The quantum dot solar cells based on Si QD are capable to outperform the bulk devices based on c-Si material due to the quantum properties, such as, the quantized energy eigen states, added density of states and corresponding absorption coefficient covering lower energy range of incident spectrum which improves the light absorption in the heterostructure for conversion in to e-h pair. In order to understand the working of QD solar cells, the mechanisms behind the performance need to be analyzed in terms of current-voltage characteristics. To this end, based on the presented theoretical framework in section 2, the current density-voltage characteristics is simulated for a Si QD/c-Si cell with respect to the number of QD layers on top of the c-Si wafer. A simplified semi-analytical approach for Si based QW solar cells is used here to describe Si QD solar cell behaviour, which depends on the complex processes between localized and extended states, such as carrier capture and escape into and from quantum confined energy levels [82]. In Fig. 7, the J_{SC} increases from 27.4 $mAcm^{-2}$ to 29.4 $mAcm^{-2}$ with addition of QD layers, N_{QD} equal to 25 (the number of layers is decided from reference [42]). This increase in current density is attributed to the increased absorption of Si QD and correspondingly improved quantum efficiency in the range of 690-1010 nm (Fig. 6). The spectral properties of photogenerated charge carriers within quantum confined energy levels have been recently studied by Aeberhard [83].

Figure 7 shows a significant shift of I_{SC} towards a higher value without any effect around V_{OC}. In the studied Si QD solar cell, V_{OC} is dependent on the ratio of generated photocurrent to the dark saturation current as described by Eq. (5). A change in V_{OC} may be related to the enhancement in

the saturation current, which is determined by various mechanisms, such as the recombination current or diffusion current. In both the cases, V_{OC} decreases with increasing temperature, as expressed below [84]:

$$V_{OC}(T) = (E_g/q) - CT \quad (20)$$

where, E_g represents the energy band gap, and C represents the temperature coefficient which has a logarithmic dependence on the intrinsic properties of the solar cell material. Equation (20) shows that the V_{OC} depends on the E_g at room temperature, which remains nearly unaffected by an increase in quantum efficiency at above bandgap energies. It indicates that V_{OC} may not change by the addition of Si nanocrystals as an active layer (on the host semiconductor, c-Si with $E_g \approx 1.1$ eV), which is supported by existing literature on Si QD solar cells [75, 85]. Wu et al. [85] reported that V_{OC} is quite insensitive to the Si nanocrystal size in a Si QD solar cell. In another report, Dutta et al. [75] have not found any change in V_{OC} by addition of Si QDs in a solar cell. However, the detailed mechanism of the dependence of V_{OC} on the quantum efficiency of a QD solar cell is not well understood [86].

4.3. Effect of illumination

Previous studies have shown that the changes in illumination affect the I_{PH}, V_{OC} and diode ideality factor, which changes the saturation current [87, 88]. The saturation current, is dependent on the illumination level (or CR) and is related to the I_{PH} and V_{OC} by following equations:

$$I_i = \frac{I_{PH}}{2[\exp(qV_{OC}/k_B n T_C) - 1]} \quad (21)$$

The value of I_r is approximated as:

$$I_r = \frac{I_{PH}}{2[\exp(qV_{OC}/k_B m T_C) - 1]} \quad (22)$$

In this case, the substitution of the values of I_i and I_r from Eq. (21) and Eq. (22) in Eq. (3) and Eq. (4) respectively, and then the values of I_{D1} and I_{D2} from Eq. (3) and Eq. (4) in Eq. (1) with the appropriate approximations ($R_S \rightarrow 0$, $R_{SH} \rightarrow \infty$ and $I \rightarrow 0$ at $V \rightarrow V_{OC}$) results in I_{PH}-I_{PH}/2-I_{PH}/2 $\rightarrow$ 0. That indicates the correctness of the approximations made for I_i and I_r through Eq. (21) and Eq. (22) respectively.

The performance parameters (I_{SC}, V_{OC}, FF and efficiency η) of the polycrystalline Si solar cell are calculated for standard test conditions and low concentration. These parameters are calculated using the theoretical framework developed in this article. The calculated performance parameters from theoretical model are listed in Table 6. With increasing CR from 1 sun to 5 suns, the short circuit current density increases from 29.4 to 147.2 mA/cm^2, the open circuit voltage increases from 0.565 V to 0.609 V and the efficiency of a Si QD solar cell decreases from 10.9% to 7.79%. A plot having simulated current-voltage curves for various CR values is shown in Fig. 8. A linear relationship between the output current of Si QD solar cell and CR is observed. This increasing trend of output current with an increase in illumination is consistent with the observation of other experimental studies for a Si solar cell [87, 88].

For a solar cell, the upper limit of achievable V_{OC} is calculated by the difference between electron and hole Fermi level as given by [89]:

$$qV_{OC} = E_{Fn} - E_{Fp} \tag{23}$$

Considering an ideal case, where the transport mechanism does not severely limit the solar cell performance, Eq. (23) can be used as a starting point to derive the achievable V_{OC}. The difference between electron and hole Fermi level gives the open-circuit voltage (V_{OC}), which increases with increasing illumination level at a constant temperature as reported in previous work [89]. A similar increasing trend of V_{OC} with CR is observed through the current-voltage

calculations for a Si QD/c-Si heterojunction solar cell as shown in Fig. 8. Previous studies have shown that the charge collection is governed by a drift mechanism near the short circuit condition and diffusion mechanism near open-circuit condition [87]. For a Si QD/c-Si heterojunction solar cell under short circuit conditions, the minority charge carrier concentration on both sides of the junction increases with a significant contribution from the quantized energy levels have charge confinement in Si QD (Fig. 2 and Fig. 4) resulting in the increase of the drift current, which depends on the number of minority carriers. Whereas under open circuit conditions, the P-N junction remains under forward bias due to the light-generated carriers on both sides of the junction, which increases the diffusion current. The balance between drift and diffusion current in opposite directions results in zero current from the Si QD solar cell under open circuit conditions. The current-voltage characteristics plotted in Fig. 8 for Si QD/c-Si heterojunction solar cell shows a shift in the value of maximum power point (P_{MAX}) towards the lower voltage side with the increase in CR. This shift in P_{MAX} at higher illumination level is mainly attributed to the enhanced recombination of carriers governed by diffusion transport in the conduction band under flat-band condition, which has been investigated for low concentration illumination in previous work [87]. The data listed in Table 6 indicate the dependence of η and FF of Si QD solar cell on the CR, which shows that efficiency decreases with increasing CR. The decrease in efficiency is mainly attributed to the reduction in FF with increasing CR. With increasing CR the recombination of charge carrier increases, which is indicated by reduction of shunt resistance in Table 6 and the finding is in accordance with the reported results [88]. The shunt resistance reduction is mainly dependent on the intensity of illumination and it may be unaffected by the addition of Si QDs. The reduction in shunt resistance is mainly due to slightly different junction capacitance behaviour of silicon solar cells

under low concentration illumination condition due to the following reasons: (1) an exponential variation in the number of minority charge carriers, and (2) occupation of the electronic DOS by excess minority charge carriers. An increase in illumination results in an introduction of excess minority carriers, with an insignificant change in the number of majority carriers in the base Si. A small change in the number of majority charge carriers leads to a minor downward shift of hole Fermi level, E_{Fp} [89]. Whereas the electron carrier density under equilibrium conditions remains negligible, therefore the electron Fermi level, E_{Fn}, changes significantly when excess carriers are injected or photogenerated at higher illumination level, which results in an exponential increase in the junction capacitance and decrease in the shunt resistance [88]. The rate of increase of V_{OC} with respect to CR, $dV_{OC}/d(CR)$ is found to decrease with increasing illumination, which may be attributed to the increase in the recombination as indicated by other researchers [90].

5. CONCLUSIONS

The Si QD solar cell is theoretically mimicked using an equivalent circuit, which accounts for the possible recombination losses under low concentration illumination. The electrical output is estimated using proposed theoretical model by considering the fundamental properties of intrinsic Si reported in the literature. It is concluded that enhanced spectral absorption is recorded due to the presence of QD layers on top of the c-Si solar cell. An increase of ~7.5% in generated short circuit current density is observed due to extra absorption of incident radiation through Si QD, which is in accordance with the experimental findings. The performance of Si QD/c-Si solar cell has been studied with respect to the low concentration illumination, wherein with increasing

CR from 1 sun to 5 suns, the short circuit current density increases from 29.4 to 147.2 mA/cm^2 and the open circuit voltage increases from 0.565 to 0.609 V.

ACKNOWLEDGEMENTS

Author acknowledges scientific discussions held with Dr. Ratna Sircar and Dr. Manoj Kumar.

REFERENCES

1. L. Korte, E. Conrad, H. Angermann, R. Stangl, M. Schmidt, Advances in a-Si:H/c-Si heterojunction solar cell fabrication and characterization, Solar Energy Materials & Solar Cells 93 (2009) 905-910.
2. Y. Zhang, N. Stokes, B. Jia, S. Fan, M. Gu, Towards ultra-thin plasmonic silicon wafer solar cells with minimized efficiency loss, Scientific Reports 4 (2014) 4939-1-6.
3. L. Wang, A. Lochtefeld, J. Han, A. P. Gerger, M. Carroll, J. Ji, A. Lennon, H. Li, R. Opila, A. Barnett, Development of a 16.8% Efficient 18-μm Silicon Solar Cell on Steel, IEEE J. Photovolt. 4 (2014) 1397-1404.
4. S. Schoenfelder, O. Breitenstein, S. Rissland, R. D. Donno, J. Bagdahn, Kerfless Wafering for Silicon Wafers by Using a Reusable Metal Layer, Energy Procedia 38 (2013) 942-949.
5. http://www.xtalsolar.com/ (accessed on 16-07-2016).
6. http://1366tech.com/technology/direct-wafer/ (accessed 16-07-2016).
7. http://www.nexwafe.com/HOME/ (accessed 16-07-2016).
8. T. Tiedle, E. Yablonovitch, G. Cody, B. Brooks, Limiting efficiency of silicon solar cells, IEEE Trans. Electron Dev. ED-31 (1984) 711-716.

9. L. Wang, J. Han, J. Ji, A. Lennon, A. Lochtefeld, A. Gerger, M. Carroll, P. Teng, R. Opila, A. Barnett, Light Trapping in an 18 μm Silicon Solar Cell with a Current Density of 34.5 mA/cm^2, International Journal of Emerging Technology and Advanced Engineering, 5 (2015) 7-15.
10. A. Ingenito, O.Isabella, M. Zeman, Experimental demonstration of $4n^2$ classical absorption limit in nanotextured ultrathin solar cells with dielectric omnidirectional backreflector, ACS Photonics 1 (2014) 270-278.
11. F. Cao, K. Chen, J. Zhang, X. Ye, J. Li, S. Zou, X. Su, Next-generation multi-crystalline silicon solar cells: Diamond-wire sawing, nano-texture and high efficiency, Solar Energy Materials & Solar Cells 141 (2015) 132-138.
12. H.A. Atwater, A. Polman, Plasmonics for improved photovoltaic devices, Nature Materials 9 (2010) 205-213.
13. S. Glunz, Photonics for high efficiency crystalline silicon solar cells, Workshop on Nanophotonics – Essential ingredient for efficient and cost-effective solar cells?, 28th European PV Solar Energy Conference and Exhibition (EU-PVSEC), Paris, 2013.
14. A. Descoeudres, Z.C. Holman, L. Barraud, S. Morel, S.D. Wolf, C. Ballif, >21% Efficient Silicon Heterojunction Solar Cells on n- and p-Type Wafers Compared, IEEE J. Photovolt. 3 (2013) 83-89.
15. A. Gupta, M. Vashistha, P. Sharma, Single junction a-Si:H solar cell with a-Si:H/nc-Si:H/a-Si:H quantum wells, Thin Solid Films 550 (2014) 643–648.
16. Y. Hayashi, D. Li, A. Ogura, Y. Ohshita, Role of i-aSi:H Layers in aSi:H/cSi Heterojunction Solar Cells, IEEE J. Photovolt. 3 (2013) 2156-3381.

17. D. Reaux, J. Alvarez, M. E. Gueunier-Farret, J. P. Kleider, Impact of Defect-pool Model Parameters on the Lifetime in c-Si/a-Si:H Heterojunction Solar Cells, Energy Procedia 77 (2015) 153-158.

18. A. Descoeudres, C. Allebé, N. Badel, L. Barraud, J. Champliaud, F. Debrot, A. Faes, A. Lachowicz, J. Levrat, S. Nicolay, L. Sansonnens, M. Despeisse, C. Ballif, Silicon Heterojunction Solar Cells: Towards Low-cost High-Efficiency Industrial Devices and Application to Low-concentration PV, Energy Procedia 77 (2015) 508-514.

19. M. Taguchi, A. Yano, S. Tohoda, K. Matsuyama, Y. Nakamura, T. Nishiwaki, K. Fujita, E. Maruyama, 24.7% Record Efficiency HIT Solar Cell on Thin Silicon Wafer, IEEE Journal of Photovoltaics, 4 (2013) 1-4.

20. G. Coletti, Y. Wu, G. Janssen, J. Loffler, B.B. Van Aken, F. Li, Y. Shen, W. Yang, J. Shi, G. Li, Z. Hu, J. Xiong, 20.3% MWT silicon heterojunction solar cell – A novel heterojunction integrated concept embedding low Ag consumption and high module efficiency, IEEE Journal of Photovoltaics 5 (2014) 55-60.

21. K. Masuko, M. Shigematsu, T. Hashiguchi, D. Fujishima, M. Kai, N. Yoshimura, T. Yamaguchi, Y. Ichihashi, T. Mishima, N. Matsubara, T. Yamanishi, T. Takahama, M. Taguchi, E. Maruyama, S. Okamoto, Achievement of More Than 25% Conversion Efficiency With Crystalline Silicon Heterojunction Solar Cell, IEEE Journal of Photovoltaics, 4 (2014) 1433-1435.

22. M.A. Green, Third Generation Photovoltaics: Advanced Solar Energy Conversion, Springer Series in Photonics, Springer, Heidelberg, 2005.

23. C. S. Solanki, G. Beaucarne, Advanced solar cell concepts, Energy for Sustainable Development, 11 (2007) 17-23.

24. K. W. J. Barnham and G. Duggan, A new approach to high-efficiency multi-band-gap solar cells, J. Appl. Phys. 67 (1990) 3490.

25. N.G. Anderson, Ideal theory of quantum well solar cells, J. Appl. Phys. 78 (1995) 1850.

26. H. Kintz, X. Paquez, O. Sublemontier, Y. Leconte, N. Herlin-Boime, C. Reynaud, Synthesis and layering of Si quantum dots/SiO2 composite films for third generation solar cells, Thin Solid Films 593 (2015) 96–101.

27. G. Conibeer, M. Green, R. Corkish, Y. Cho, E. C. Cho, C. W. Jiang, T. Fangsuwannarak, E. Pink, Y. Huang, T. Puzzer, T. Trupke, B. Richards, A. Shalav, K.L. Lin, Silicon nanostructures for third generation photovoltaic solar cells, Thin Solid Films 511-512 (2006) 654.

28. G. Conibeer, M. Green, E. C. Cho, D. König, Y. H. Cho, T. Fangsuwannarak, G. Scardera, E. Pink, Y. Huang, T. Puzzer, S. Huang, D. Song, C. Flynn, S. Park, X. Hao, D. Mansfield, Silicon quantum dot nanostructures for tandem photovoltaic cells, Thin Solid Films 516 (2008) 6748.

29. L. V. Dao, J. Davis, P. Hannaford, Y. H. Cho, M. A. Green, E. C. Cho, Ultrafast carrier dynamics of Si quantum dots embedded in SiN matrix, Appl. Phys. Lett. 90 (2007) 081105.

30. D. Song, E. C. Cho, G. Conibeer, Y. Huang, M. A. Green, Fabrication and electrical characteristics of Si nanocrystal/c-Si heterojunctions, Appl. Phys. Lett. 91 (2007) 123510.

31. R. Rölver, B. Berghoff, D.L. Bätzner, B. Spangenberg, H. Kurz, Lateral Si/SiO2 quantum well solar cells, Appl. Phys. Lett. 92 (2008) 212108.

32. B. Stegemann, A. Schoepke, M. Schmidt, Structure and photoelectrical properties of $SiO_2/Si/SiO_2$ single quantum wells prepared under ultrahigh vacuum conditions, J. Non-Cryst. Solids 354 (2008) 2100.

33. T. Kirchartz, K. Seino, J. M. Wagner, U. Rau, F. Bechstedt, Efficiency limits of Si/SiO2 quantum well solar cells from first-principles calculations, J. Appl. Phys. 105 (2009) 104511.

34. M. M. Rahman, M. Y. Lee, Y. C. Tsai, A. Higo, H. Sekhar, M. Igarashi, M. E. Syazwan, Y. Hoshi, K. Sawano, N. Usami, Y. Li, S. Samukawa, Impact of silicon quantum dot super lattice and quantum well structure as intermediate layer on p-i-n silicon solar cells, Prog. Photovolt: Res. Appl. (2015) DOI: 10.1002/pip.2726.

35. U. Aeberhard, Microscopic theory and numerical simulation of quantum well solar cells, SPIE Proc. on Physics and Simulation of Optoelectronic Devices XVIII 7597 (2010) 759702.

36. U. Aeberhard, R. Morf, Microscopic nonequilibrium theory of quantum well solar cells, Phys. Rev. B 77 (2008) 125343.

37. J.W. Luo, P. Stradins, A. Zunger, Matrix-embedded silicon quantum dots for photovoltaic applications: a theoretical study of critical factors, Energy Environ. Sci. 4 (2011) 2546-2557.

38. P.J. Walters, G.I. Bourianoff, H.A. Atwater, Field-effect electroluminescence in silicon nanocrystals, Nature Materials 4 (2005) 143-146.

39. L. Pavesi, L.D. Negro, C. Mazzoleni, G. Franzo, F. Priolo, Optical gain in silicon nanocrystals, Nature 408 (2000) 440-444.

40. M. Cazzanelli, D. Navarro-Urriós, F. Riboli, N. Daldosso, L. Pavesi, J. Heitmann, L.X. Yi, R. Scholz, M. Zacharias, U. Gösele, J. Appl. Phys. 96 (2004) 3164-3171.

41. G. Conibeer, Third-generation photovoltaics, Materials Today 10 (2007) 42-50.

42. E.C. Cho, M.A. Green, G. Conibeer, D. Song, Y.H. Cho, G. Scardera, S. Huang, S. Park, X. J. Hao, Y. Huang, L.V. Dao, Silicon Quantum Dots in a Dielectric Matrix for All-Silicon Tandem Solar Cells, Advances in OptoElectronics 2007 (2007) 69578-1-11.

43. P.G. Kale, C.S. Solanki, Silicon quantum dot solar cell using top-down approach, Int. Nano Lett. 5 (2015) 61-65.

44. H. Kintz, X. Paquez, O. Sublemontier, Y. Leconte, N. Herlin-Boime, C. Reynaud, Synthesis and layering of Si quantum dots/SiO_2 composite films for third generation solar cells, Thin Solid Films 593 (2015) 96-101.

45. Z. Zhou, R.A. Friesner, L. Brus, Electronic Structure of 1 to 2 nm Diameter Silicon Core/Shell Nanocrystals: Surface Chemistry, Optical Spectra, Charge Transfer, and Doping, J. Am. Chem. Soc. 125 (2003) 15599-15607.

46. E.C. Cho, S. Park, X. Hao, D. Song, G. Conibeer, S.C. Park, M.A Green, Silicon quantum dot/crystalline silicon solar cells; Nanotechnology 19 (2008) 245201-1-5.

47. E.G. Barbagiovanni, D. J. Lockwood, P.J. Simpson, L.V. Goncharova, Quantum confinement in Si and Ge nanostructures: Theory and experiment, Applied Physics Reviews 1 (2014) 011302-1-47.

48. P. Löper, D. Stüwe, M. Künle, M. Bivour, C. Reichel, R. Neubauer, M. Schnabel, M. Hermle, O. Eibl, S. Janz, M. Zacharias, S. W. Glunz, A Membrane Device for Substrate-Free Photovoltaic Characterization of Quantum Dot Based p-i-n Solar Cells, Advanced Materials 24 (2012) 3124-3129.

49. P. Löper, R. Müller, D. Hiller, T. Barthel, E. Malguth, S. Janz, J. C. Goldschmidt, M. Hermle, M. Zacharias, Quasi-Fermi-level splitting in ideal silicon nanocrystal superlattices, Physical Review B 84 (2011) 195317/1-6.

50. J. E. Garland, D. J. Crain, J. P. Zheng, C. M. Sulyma, D. Roy, Electro-analytical characterization of photovoltaic cells by combining voltammetry and impedance spectroscopy: voltage dependent parameters of a silicon solar cell under controlled illumination and temperature, Energ. Environ. Sci 4 (2011) 485-498.

51. D. Ding, S.R. Johnson, S.Q. Yu, S.N. Wu, Y.H. Zhang, A semi-analytical model for semiconductor solar cells, J. Appl. Phys. 110 (2011) 123104.

52. P. Yadav, B. Tripathi, K. Pandey, M. Kumar, Investigating the charge transport kinetics in poly-crystalline silicon solar cells for low-concentration illumination by impedance spectroscopy, Solar Energy Materials & Solar Cells 133 (2015) 105-112.

53. C.T. Sah, R.N. Noyce, W. Shockley, Carrier Generation and Recombination in P-N Junctions and P-N Junction Characteristics, Proceedings of the IRE 45 (1957) 1228 – 1243.

54. K. Ishaque, Z. Salam, H. Taheri, A. Shamsudin, A critical evaluation of EA computational methods for Photovoltaic cell parameter extraction based on two diode model, Solar Energy 85 (2011) 1768-1779.

55. T. Kirchartz, Generalized Detailed Balance Theory of Solar Cells, Forschungszentrum Jülich, 2009.

56. J.C. Rimada, L. Hernandez, Modelling of ideal AlGaAs quantum well solar cells, Microelectronics Journal 32 (2001) 719-723.

57. S. J. Lade, A. Zahedi, A revised model for AlGaAs/GaAs quantum well solar cells, Microelectronics Journal 35 (2004) 401-410.

58. Reference solar spectral irradiance Air Mass 1.5, American Society for Testing, Materials (ASTM), http://rredc.nrel.gov/solar/spectra/am1.5/ (accessed on 13-01-2015).

59. M. A. Green, M. J. Keevers, Optical Properties of Intrinsic Silicon at 300 K, Progress in Photovoltaics: Research and Applications 3 (1995) 189-192.

60. C.S. Solanki, Solar Photovoltaics: Fundamentals, Technologies and Applications, PHI Learning Pvt. Ltd., New Delhi, 2011.

61. O. Breitenstein, Nondestructive local analysis of current-voltage characteristics of solar cells by lock-in thermography, Solar Energy Materials & Solar Cells 95 (2011) 2933-2936.

62. S.K. Saha, A.M. Farhan, S.I. Reba, S.I. Ferdaus, M.I.B. Chowdhury, An analytical model of dark saturation current of silicon solar cell considering both SRH and Auger recombination, Micro and Nanoelectronics (RSM), 2011 IEEE Regional Symposium 2011. http://dx.doi.org/10.1109/RSM.2011.6088280.

63. C.W. Jiang, M.A. Green, Silicon quantum dot superlattices: Modeling of energy bands, densities of states, and mobilities for silicon tandem solar cell applications, J. Appl. Phys. 99 (2006) 114902.

64. M.I. Vexler, S.E. Tyaginov and A.F. Shulekin, Determination of the hole effective mass in thin silicon dioxide film by means of an analysis of characteristics of a MOS tunnel emitter transistor, J. Phys.: Condens. Matter 17 (2005) 8057-8068.

65. M.G. Mavros, Computing the optical properties of doped silicon quantum dots for photovoltaic application, Honours Thesis, University of Florida, 2011.

66. S. L. Chuang, Physics of Optoelectronic Devices, Wiley-Interscience publication, New York, 1995.

67. S. Takeoka, M. Fujii and S. Hayashi, Size-dependent photoluminescence from surface-oxidized Si nanocrystals in a weak confinement regime, Phys. Rev. B: Condens. Matter 62 (2000) 16820.

68. W.B. Jackson, S.M. Kelso, C.C. Tsai, J.W. Allen, S. J. Oh, Energy dependence of the optical matrix element in hydrogenated amorphous and crystalline silicon, Phys. Rev. B 31 (1985) 5187.

69. B. G. Lee, D. Hiller, J. W. Luo, O. E. Semonin, M. C. Beard, M. Zacharias, P. Stradins, Strained Interface Defects in Silicon Nanocrystals, Advanced Functional Materials 22 (2012) 3223-3232.

70. S. Mirabella, R. Agosta, G. Franzò, I. Crupi, M. Miritello, R. L. Savio, M. A. D. Stefano, S. D. Marco, F. Simone, A. Terrasi, Light absorption in silicon quantum dots embedded in silica, Journal of Applied Physics 106 (2009) 103505/1-8.

71. S.K. Saha, A.M. Farhan, S.I. Reba, S.I. Ferdaus, M.I.B. Chowdhury, An analytical model of dark saturation current of silicon solar cell considering both SRH and Auger recombination, Micro and Nanoelectronics (RSM), 2011 IEEE Regional Symposium 2011. http://dx.doi.org/10.1109/RSM.2011.6088280.

72. W. Gerlach, H. Schlangenotto, H. Maeder, On the radiative recombination rate in silicon, Phys. Status Solidi A 13 (1972) 277-283.

73. A.B. Sproul, M.A. Green, Improved value for the silicon intrinsic carrier concentration from 275 to 375 K, J. Appl. Phys. 70 (1991) 846.

74. A. Zunger, L.W. Wang, Theory of silicon nanostructures, Applied Surface Science 102 (1996) 350-359.

75. M. Dutta, L. Thirugnanam, P.V. Trinh, N. Fukata, High Efficiency Hybrid Solar Cells Using Nanocrystalline Si Quantum Dots and Si Nanowires, ACS Nano 9 (2015) 6891-6899.

76. W.L. Wilson, P.F. Szajowski, L.E. Brus, Quantum Confinement in Size-Selected, Surface-Oxidized Silicon Nanocrystals, Science 262 (1993) 1242-1244.

77. G. G. Younise, Modeling and Analysis of Homojunction Silicon Solar Cell, Jou. Raf. Sci. 22 (2011) 72-79.

78. M. Paxman, J. Nelson, B. Braun, J. Connolly, K.W.J. Barnham, Modeling the spectral response of the quantum well solar cell, J. Appl. Phys. 74 (1993) 614-621.

79. A. Laha, E. Bugiel, R. Dargis, D. Schwendt, M. Badylevich, V.V. Afanasev, A. Stesmans, A. Fissel, H.J. Osten, Integration of low dimensional crystalline Si into functional epitaxial oxides, Microelectronics Journal 40 (2009) 633-637.

80. A.K. Panchal, C.S. Solanki, Post deposition annealing temperature effect on silicon quantum dots embedded in silicon nitride dielectric multilayer prepared by hot-wire chemical vapor deposition, Thin Solid Films 517 (2009) 3488-3491.

81. S. Park, E. Cho, D. Song, G. Conibeer, M. A.Green, n-Type silicon quantum dots and p-type crystalline silicon heteroface solar cells, Solar Energy Materials & Solar Cells 93 (2009) 684-690.

82. U. Aeberhard, Theory and simulation of quantum photovoltaic devices based on the non-equilibrium Green's function formalism, J. Comput. Electron. 10 (2011) 394-413.

83. U. Aeberhard, Spectral properties of photogenerated carriers in quantum well solar cells, Solar Energy Materials & Solar Cells 94 (2010) 1897-1902.

84. S. M. Sze, Physics of Semiconductor Devices, John Wiley & Sons, 1981.

85. P.J. Wu, Y.C. Wang, I.C. Chen, Fabrication of Si heterojunction solar cells using P-doped Si nanocrystals embedded in SiNx films as emitters, Nanoscale Research Letters 8 (2013) 457/1-7.

86. T. Tayagaki, Y. Hoshi, N. Usami, Investigation of the open-circuit voltage in solar cells doped with quantum dots, Scientific Reports 3 (2013) 2703/1-5.

87. P. Yadav, B. Tripathi, K. Pandey, M. Kumar, Investigating the charge transport kinetics in poly-crystalline silicon solar cells for low-concentration illumination by impedance spectroscopy, Solar Energy Materials & Solar Cells 133 (2015) 105-112.

88. P. Yadav, B. Tripathi, K. Pandey, M. Kumar, Recombination kinetics in silicon solar cell under low-concentration: Electro-analytical characterization of space-charge and quasi-neutral regions, Phys. Chem. Chem. Phys. 16 (2014) 15469-15476.

89. I. Mora-Sero, G. Garcia-Belmonte, P.P. Boix, M.A. Vazquez, J. Bisquert, Impedance spectroscopy characterization of highly efficient silicon solar cells under different light illumination intensities, Energ. Environ. Sci. 2 (2009) 678–686.

90. S. Banerjee, W.A. Anderson, Electron irradiation effects on the shunt resistance of silicon solar cells, Solar Cells 20 (1987) 315-321.

ACCEPTED MANUSCRIPT

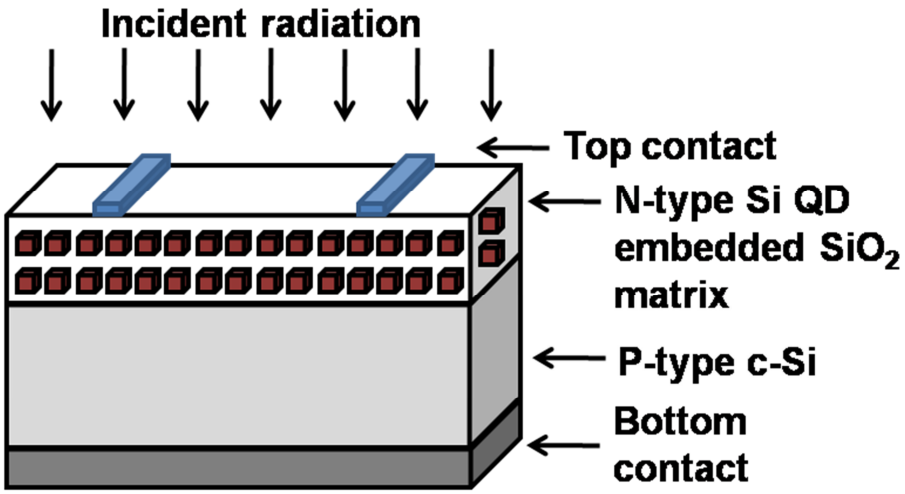

Figure 1: Schematic diagram of theoretically modeled silicon quantum dot/crystalline silicon solar cell.

ACCEPTED MANUSCRIPT

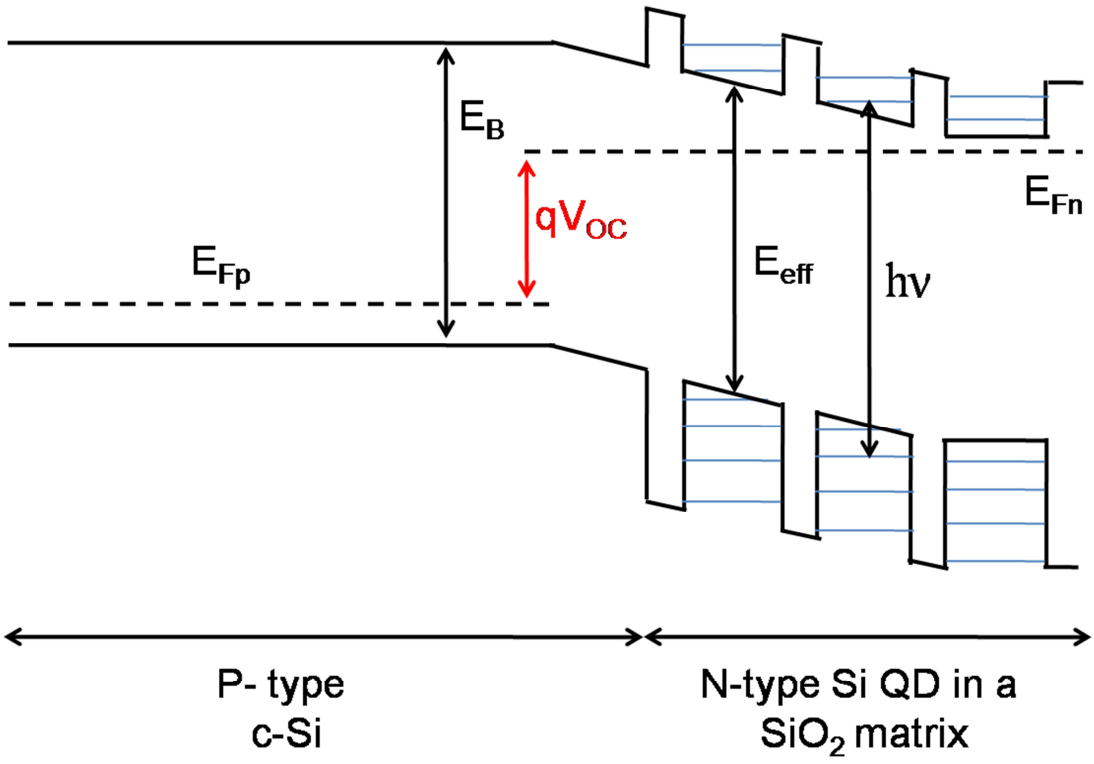

Figure 2: Schematic representation of N-type Si quantum dots (QD) incorporated SiO_2 matrix on top of the solar cell.

ACCEPTED

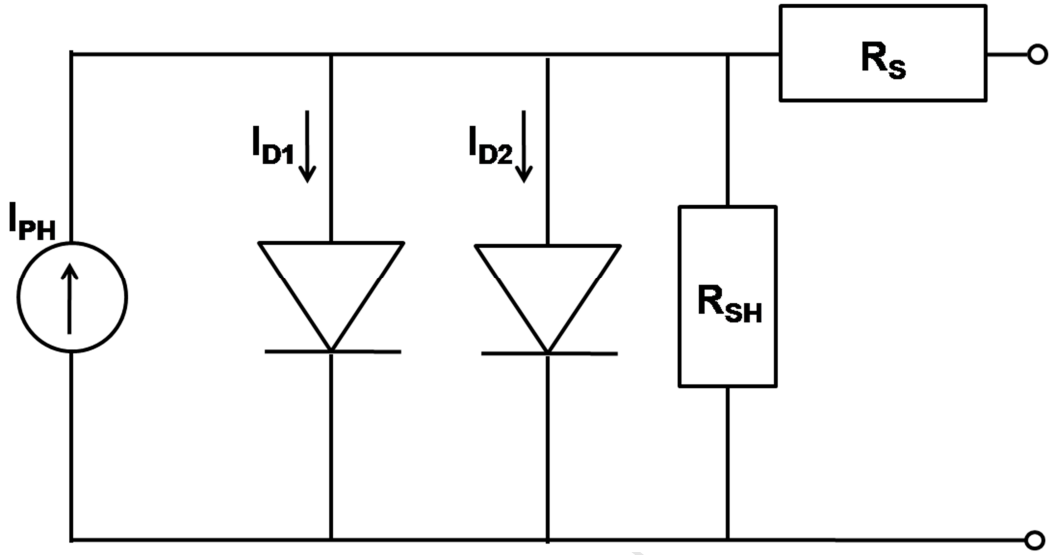

Figure 3: Diode equivalent circuit of Si quantum dot solar cell using two-diode model [52].

ACCEPTED MANUSCRIPT

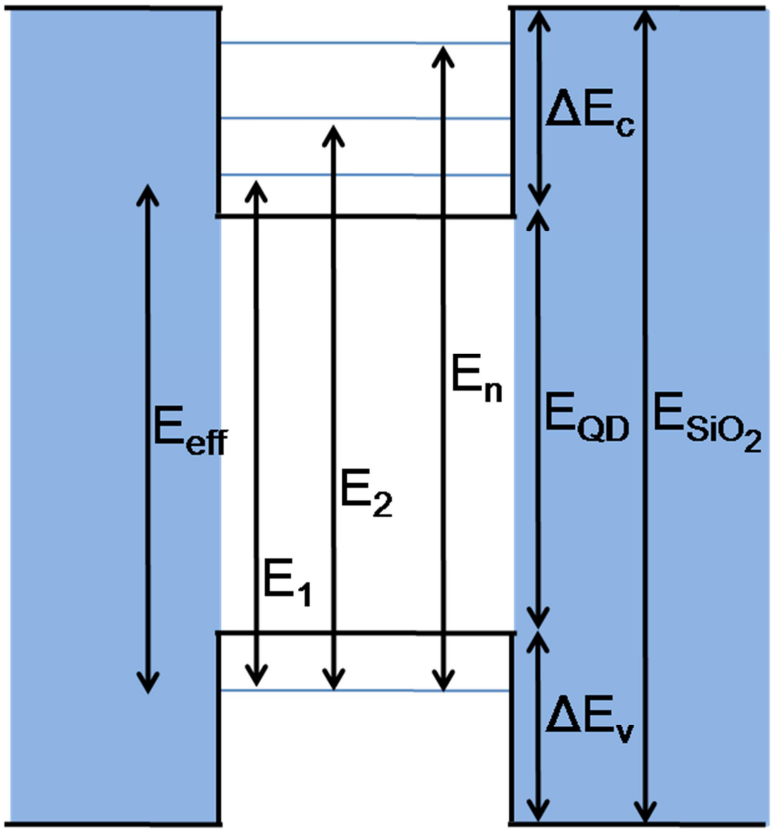

Figure 4: Band diagram of a Si QD (SiO_2)/c-Si with SiO_2 band gap (E_{SiO_2}), Si QD band gap (E_{QD}), effective band gap of QD (E_{eff}), conduction band offset (ΔE_c), conduction band energy levels (E_1 to E_n) and valence band offset (ΔE_v).

ACCEPTED MANUSCRIPT

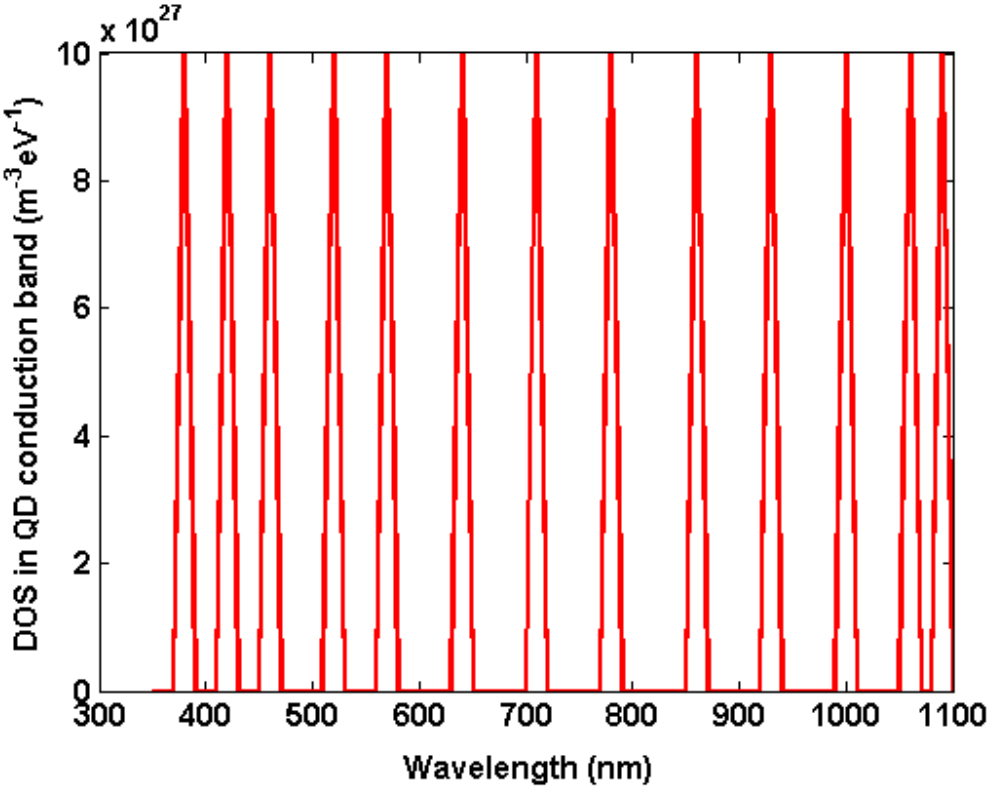

Figure 5: Calculated density of states in QD conduction band with respect to the wavelength (wavelength corresponds to the QD conduction band energy levels with reference to ground energy level of the holes).

ACCEPTED MANUSCRIPT

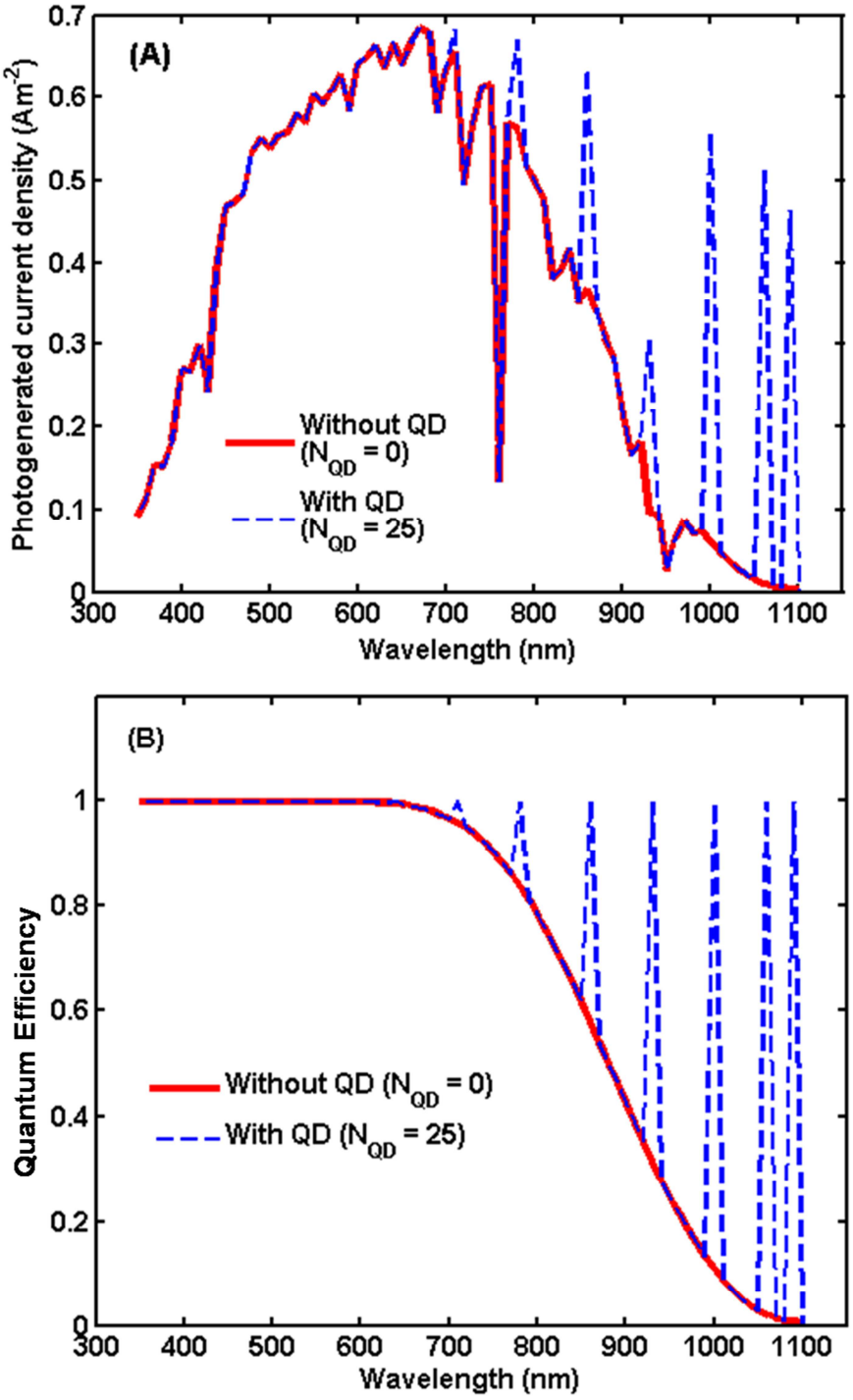

Figure 6: (A) Photogenerated current density and (B) Quantum efficiency with respect to wavelength of incident photon and variation in number of QD layers (N_{QD}).

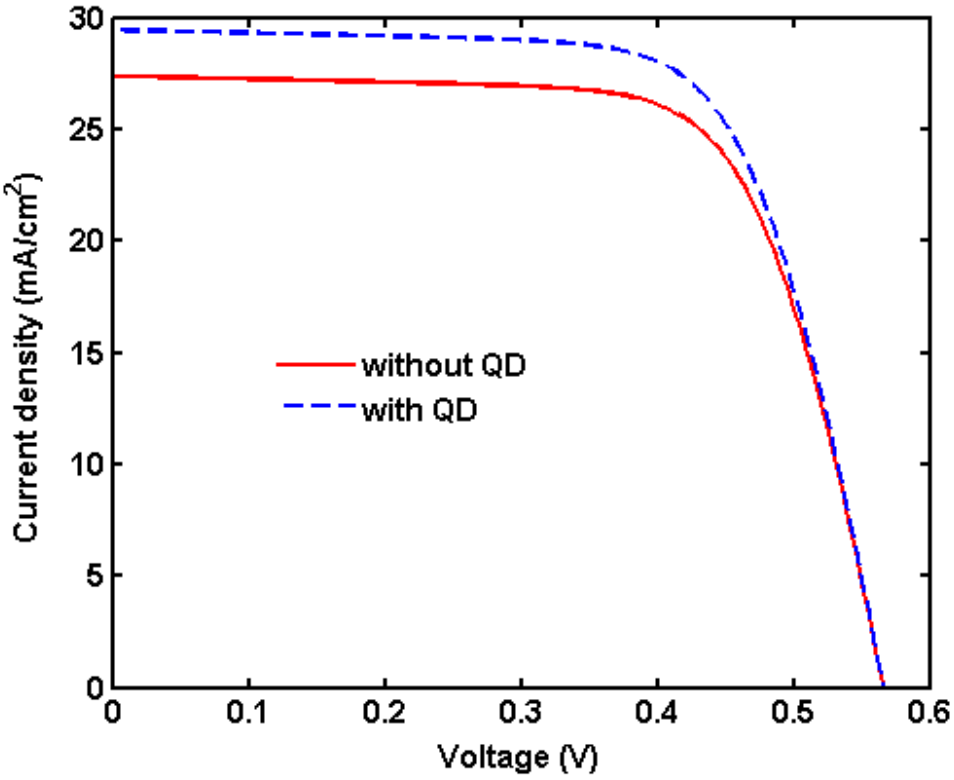

Figure 7: Current-voltage characteristics of a silicon QD/c-Si heterojunction solar cell.

ACCEPTED MANUSCRIPT

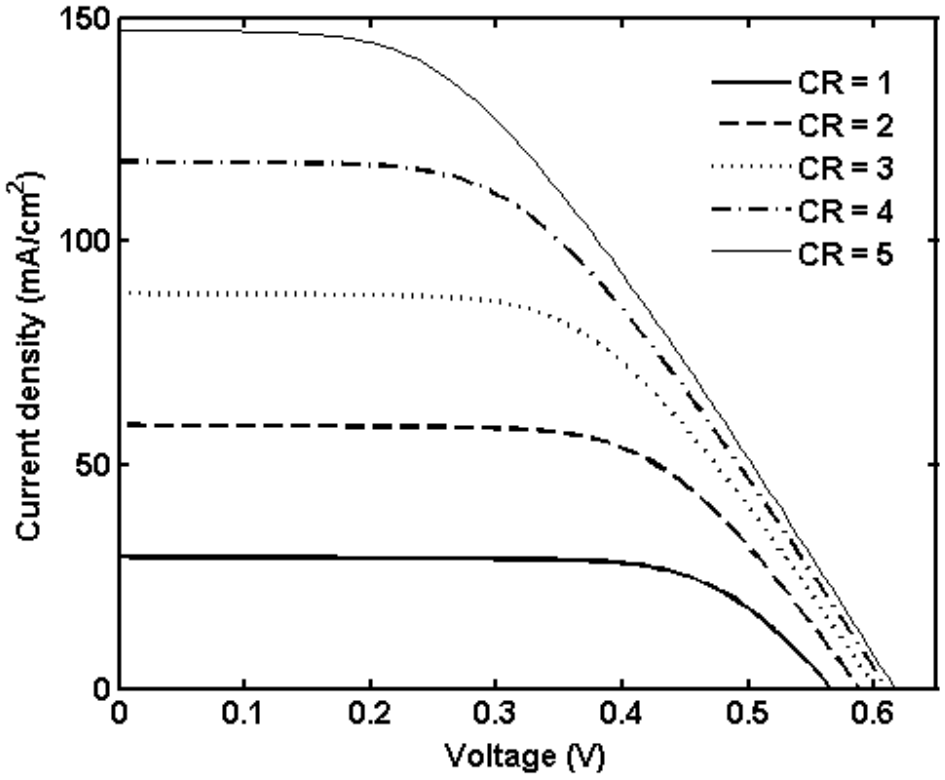

Figure 8: Current-voltage characteristics of a Si QD/c-Si heterojunction solar cell under low concentration illumination for various CR values.

ACCEPTED MANUSCRIPT

Table 1: Parameters used for calculating the DOS and absorption coefficient

Parameter	**Value**
E_{SiO_2}	9.0 eV [27]
E_{QD}	1.1 eV [27]
ΔE_c	3.2 eV [27]
ΔE_v	2.3 eV [27]
m_0	9.1×10^{-31} kg
m^*_{Be}	0.86 m_0 [42]
m^*_{Bh}	0.33 m_0 [64]
m^*_{We}	1.08 m_0 [15]
m^*_{Wh}	0.57 m_0 [15]

ACCEPTED MANUSCRIPT

Table 2: Calculated values of energy levels for the Si QD size ($L_x \times L_y \times L_z$) of $5 \times 5 \times 5$ nm^3 in SiO_2 matrix.

Energy levels	Values (eV)
E1	0.0125
E2	0.0518
E3	0.1165
E4	0.2071
E5	0.3232
E6	0.465
E7	0.6324
E8	0.8251
E9	1.042
E10	1.2845
E11	1.551
E12	1.8405
E13	2.152
E14	2.483
E15	2.83
E16	3.167

ACCEPTED MANUSCRIPT

Table 3: List of parameters used for the calculation of the absorption coefficient

Parameter	**Value**
Q	1.6×10^{-19} C
n_r	3.96
C	3×10^{8} m/s
ε_0	8.854×10^{-12} F/m
$\left\|\hat{e}.\vec{P}_{CV}\right\|^2$	2.068×10^{-49} (kg m/s)^2 [68]
$\hbar$	1.054×10^{-34} Js

ACCEPTED MANUSCRIPT

Table 4: Parameters used to calculate β, r_R, α and r_{NR}.

Parameter	**Value**
B	1.1×10^{14} cm^3/s [20]
n_i	1.1×10^{10} cm^{-3} [21]
ΔE	7.9 eV [27]
n	1.2
m	2.5
A	10-100 ms^{-1} [74]

ACCEPTED MANUSCRIPT

Table 5: Parameters used in the calculation of current-voltage characteristics of solar cell

Parameter	**Value**
V_{OC}	0.545 V
R_S	2 Ω
R_{SH}	800 Ω
I_i	3.441×10^{-10} Acm^{-2}
I_r	3.203×10^{-6} Acm^{-2}

ACCEPTED MANUSCRIPT

Table 6: The parameters extracted from I-V characteristics for an area of 1 cm^2 at 300 K.

CR	I_{SC} (mA)	V_{OC} (V)	FF (%)	η (%)	R_{SH} (Ω)	$dV_{OC}/d(CR)$
1	29.4	0.565	65.6	10.9	777	-
2	58.9	0.585	61.0	10.5	763	0.020
3	88.3	0.601	54.6	9.65	741	0.016
4	117.8	0.605	48.8	8.70	701	0.004
5	147.2	0.609	43.4	7.79	606	0.004

ACCEPTED MANUSCRIPT

ACCEPTED MANUSCRIPT

Highlights:

- Silicon based quantum dot solar cell's electrical performance evaluated.
- Equivalent circuit based I-V model for silicon quantum dot solar cell.
- Quantum efficiency of Si QD/c-Si solar cell modelled.
- Performance evaluation of Si QD/c-Si solar cell under low concentration.

ACCEPTED MANUSCRIPT